ISSN 1392–1207. MECHANIKA. 2017 Volume 23(5): 653–660

Numerical Analysis of Thermal and Hydro Dynamical Processes in Lower Fuel Channel Part of Boiling Water Reactor

L. PAUKŠTAITIS*, S. KILIKEVIČIUS, J. GUDZINSKAS***, M. GYLYS****, V. LUKOŠEVIČIUS*****
**Kaunas University of Technology, Studentų 56, LT–51424, Kaunas, Lithuania, E–mail: linas.paukstaitis@ktu.lt*
***Kaunas University of Technology, Studentų 56, LT–51424, Kaunas, Lithuania, E–mail: sigitas.kilikevicius@ktu.lt*
****Kaunas University of Technology, Studentų 56, LT–51424, Kaunas, Lithuania, E–mail: juozas.gudzinskas@ktu.lt*
*****Kaunas University of Technology, Studentų 56, LT–51424, Kaunas, Lithuania, E–mail: martynas.gylys@ktu.lt*
******Kaunas University of Technology, Studentų 56, LT–51424, Kaunas, Lithuania, E–mail: valdas.lukosevicius@ktu.lt*

crossref http://dx.doi.org/10.5755/j01.mech.23.5.16457

1. Introduction

Ignalina nuclear power plant (INPP) contains two RBMK-1500 reactors [1] which are the last modification of the modernized soviet design channel type reactor RBMK-1000 [2]. The main design features of the RBMK reactors are as follows: graphite is used as a main moderator; coolant (water and water – steam mixture) flows inside the vertical technological (fuel) channels, which are mounted in the graphite holes; fuel assemblies (bundles) are placed inside the fuel channels.

This paper presents the results of the numerical investigation of the thermal and hydro dynamical processes, which take place inside the lower part of the fuel channels during the hydro and thermal interaction between the coolant and fuel bundles.

Design of the fuel elements of the RBMK and BWR [3, 4] reactors has a lot of common features. For example, the cladding of the both reactors are made of zirconium – niobium alloy; outside diameter of the cladding tubes is similar (12 and 13.5 mm); fuel enrichment by uranium 235 varies from 2% up to 2.6% for RBMK reactor, and from 2.2% to 3% for BWR reactor, and etc. However, the fuel assemblies (bundles) of the RBMK and BWR reactors have different design. The fuel assembly of the BWR reactor has a quadratic cross section and usually consists of the 64 fuel elements. The fuel assembly of the RBMK reactor has 18 fuel elements placed in two concentric circles around the central rod inside the round fuel channel (Fig. 1). The inner diameter of the fuel channel is 80 mm, the outer diameter is 88 mm; the height of the active part of the fuel assembly is 6.86 m. The central rod is made of zirconium and niobium (2.5%) alloy and has a diameter equal to 15 mm. The fuel assembly consists of two fuel bundles, which are staked to each other and to the central rod. Between two fuel bundles there is no nuclear fuel; therefore, nuclear fission does not occur there.

The lower part of the fuel assembly (lower bundle) has 10 distance grids – spacers (Fig. 2, a).

The upper part of the fuel assembly (upper bundle) has 10 distance grids (Fig. 2, a) and 30 special grids (Fig. 2, b) for the heat transfer intensification - intensifiers. The intensifiers force to spin a coolant flow, increasing its turbulence and raising heat transfer intensity as well.

The RELAP, CATHARE, ATHLET and other program codes allow one–dimensional modelling of the coupled behaviour of the reactor's coolant system and the core for various operational and accidental conditions. However, those codes apply simplified one-dimensional nodal schemes for the flow of the coolant [6-8]. Besides that, the most works related to the numerical investigation of the coolant flow inside the channels of the complicated configuration are based on the simplified two-dimensional model of the coolant flow [9-15]. A numerical simulation (subchannel and CFD analysis) and an experimental investigation were applied mostly for the calculation of the thermal and hydrodynamic processes of the BWR [16-20,24] but not for the channel type reactor RBMK-1500.

The obtained results help better to understand the processes which have a direct influence on the reactor safety. Information about the peculiarities of steam generation process inside the fuel channel (temperature change, pressure drop, flow velocity, steam mass fraction) enables to identify the most loaded points of the fuel channel and to make necessary design and operational improvements (location of spacers and intensifiers; core loading and etc.). The results can be used for predicting of hydrogen formation process and for the forecast of the decrease of zirconium alloy strength.

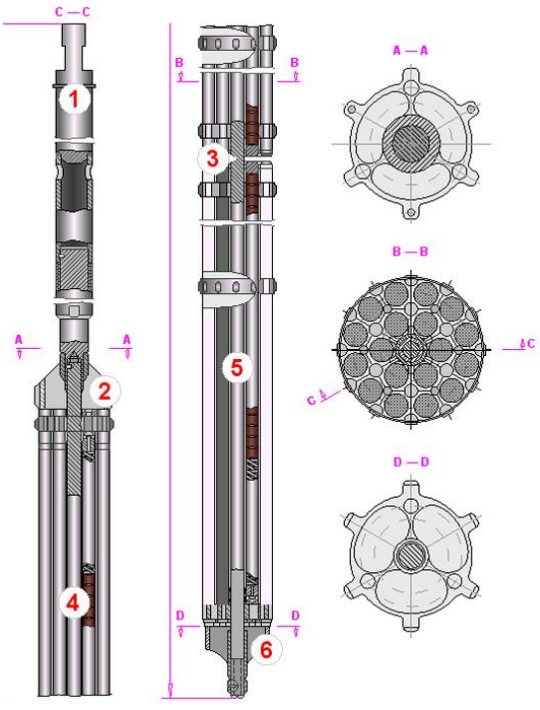

Fig. 1 Fuel assembly of the reactor RBMK-1500 [1, 2]. *1* - hanger; *2* - guide shank; *3* - carrying bar; *4* - upper fuel bundle; *5* - lower fuel bundle; *6* - tip

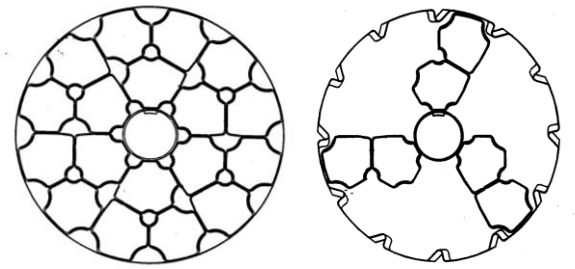

a b

Fig. 2 Distance grid – spacer (a) and heat transfer intensification grid – intensifier (b) of the fuel assembly of the reactor RBMK-1500 [5]

2. Numerical model of the fuel channel of the reactor RBMK-1500

In this work, a numerical simulation of the RBMK-1500 reactor fuel channel was made applying ANSYS CFX [21, 22], which is based on the finite volume method.

The following equations are included in the ANSYS CFX code:

- momentum conservation equations:

$$\nabla\left(\rho\vec{w}u-\mu_{ef}\nabla u\right)=-\frac{\partial p}{\partial x}+S_C-S_p^u u\,, \tag{1}$$

$$\nabla\left(\rho\vec{w}v-\mu_{ef}\nabla v\right)=-\frac{\partial p}{\partial y}+S_C-S_p^u v\,, \tag{2}$$

$$\nabla\left(\rho\vec{w}w-\mu_{ef}\nabla w\right)=-\frac{\partial p}{\partial z}+S_C-S_p^u w\,; \tag{3}$$

- mass continuity equation:

$$\nabla\left(\rho\vec{w}\right)=0\,; \tag{4}$$

- energy conservation equation:

$$\frac{\partial(\rho h)}{\partial t}+\nabla\left(\rho U h\right)=\nabla\left(\lambda\nabla T\right)+\tau:\nabla U+S_E\,, \tag{5}$$

here ρ is density, kg/m^3; h is enthalpy, J/kg; u, v, w are velocity, m/s; T is temperature, K; μ is viscosity, Pa·s; S is source; t is time, s.

One of the most difficult problems in the turbulence modelling is to ensure accurate simulation results. Therefore, the k-ε turbulence model [25], as more applicable for the modelling at the low fluid flow velocity, was applied for the numerical 3D simulation of the fuel channel of the RBMK-1500 reactor. According to the k-ε model, the turbulence viscosity is connected to the kinetic energy of the turbulence and energy dissipation via the following equation:

$$\mu_t=C_\mu\rho\frac{k^2}{\varepsilon}\,, \tag{6}$$

here C_μ is the constant which is equal to 0.09.

k and ε are the values calculated directly from the differential equations of the momentum conservation:

$$\frac{\partial(\rho k)}{\delta t}+\nabla\left(\rho U k\right)=\nabla\left(\left(\mu+\frac{\mu_t}{\sigma_k}\right)\nabla k\right)+$$
$$+P_k+P_{kb}-\rho\varepsilon, \tag{7}$$

$$\frac{\partial(\rho\varepsilon)}{\delta t}+\nabla\left(\rho U\varepsilon\right)=\nabla\left(\left(\mu+\frac{\mu_t}{\sigma_\varepsilon}\right)\nabla\varepsilon\right)+$$
$$+\frac{\varepsilon}{k}\left(C_{\varepsilon1}\left(P_k+P_{\varepsilon b}\right)-C_{\varepsilon2}\rho\varepsilon\right), \tag{8}$$

where $C_{\varepsilon1}$, $C_{\varepsilon2}$, σ_k are the constants (1.4, 1.9 and 1.3, respectively); P_k is the intensity of the turbulence influenced by the viscosity forces.

The three-dimensional geometrical model (Fig. 3) of the RBMK-1500 reactor fuel assembly (bundle) was created using SOLIDWORKS [23] and imported in ANSYS CFX, where the required boundary and initial conditions along with the assumed energy release law were set. In order to create a CFX mesh, a tetrahedral finite element type was chosen. The influence of CFX mesh density on the results was rated by changing a quantity of elements from 5 to 12 million (Table 1).

Table 1

Mesh density influence on the coolant's temperature, pressure loses and steam mass fraction

Number of elements	Temperature at outlet, °C	Pressure loses, Δp, MPa	Steam mass fraction
$5.0\cdot10^6$	279.8	0.550	37
$6.0\cdot10^6$	279.9	0.545	37
$7.0\cdot10^6$	279.9	0.540	35
$9.0\cdot10^6$	279.9	0.543	33
$10.0\cdot10^6$	279.9	0.533	30
$12.0\cdot10^6$	279.9	0.533	30

The difference between the results of 10 and 12 million elements was insignificant, therefore the quantity of 10 million elements was applied in further calculations. The numerical investigation included the estimation of the coolant's temperature distribution along and across the channel, localization of the steam generation places, establishing of the coolant velocity, steam fraction distribution and etc.

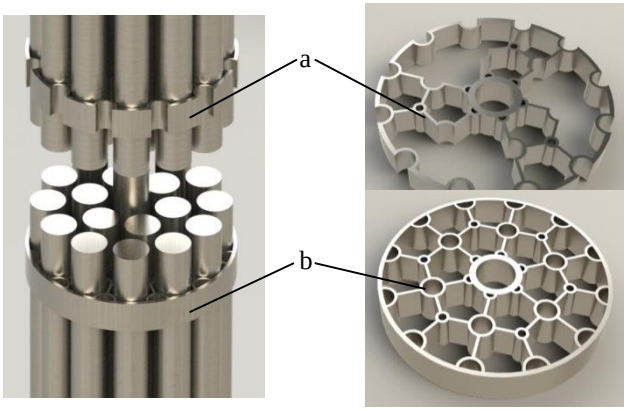

Fig. 3 Geometrical model of the fuel assembly of the RBMK-1500 reactor: (a) grid for heat transfer intensification – intensifier; (b) distance grid – spacer

An assumption was made that an axial power distribution corresponds to the cosine's law:

$$q = \frac{Q}{F}\ k_z\ cos\left(\frac{\pi\ Y}{H}\right), \tag{9}$$

here Q is the thermal power of the fuel channel, W; F is area of the heated surface; H is the length of the fuel assembly, m; Y is the coordinate, m; k_z is the heat release peaking factor by the core height (k_z = 1.511).

The following conditions were assumed in the model: coolant parameters at the inlet to the fuel channel: 263.8 C temperature; 7 MPa pressure; 5.12 kg/s flow rate; 2.605 MW power of the fuel assembly.

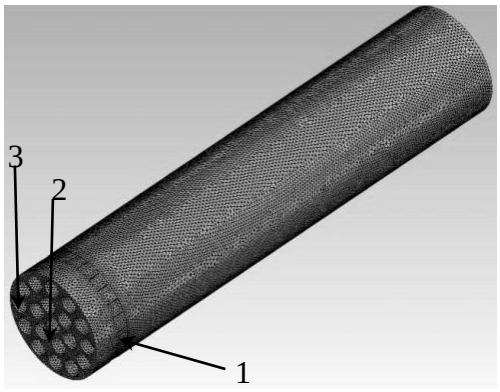

Fig. 4 Mesh grid of the fuel assembly: *1* - mesh around distance grid; *2* - fuel element; *3* - outer wall of the fuel elements

It was assumed that the heat exchange between the outside wall of the channel and the graphite moderator does not exist. For the modelling of the heat transfer process a homogeneous model of the heat transfer (HEM) was established; for the modelling of the coolant flow regime the *k-ε* turbulence model was used. The mesh grid of the fuel assembly (Fig. 4) consisted of $10 \cdot 10^6$ elements, as it was mentioned before.

The 3D model of the fuel channel of the RBMK-1500 reactor allowed a numerical investigation of the thermal and hydrodynamic processes inside the channel. Those processes were estimated at the *13* points of the fuel channel's cross section (Fig. 5).

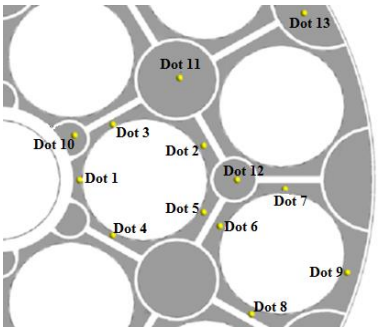

Fig. 5 Position of the check points in the cross section of the channel

There were clarified changes of the flow velocity, pressure, temperature and steam fraction.

2. Coolant flow parameters variation along the fuel channel

Fig. 6 shows a change of the coolant temperature at the height 1750 – 2450 mm of the fuel channel.

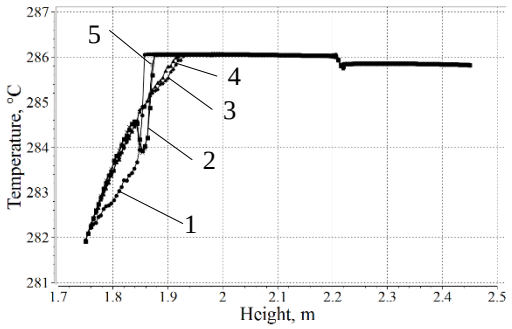

a

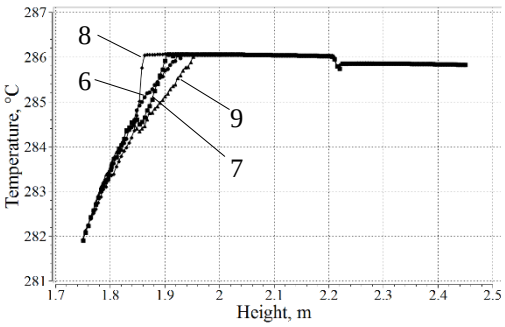

b

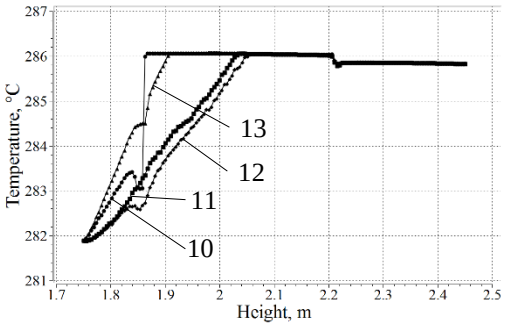

c

Fig. 6 Temperature change along the fuel channel: (a) at the *1 – 5* points; (b) at the *6 – 9* points; (c) at the *10 – 13* points

It was noticed that the coolant reached the saturation temperature before the 2.0 m height at all the points except points *11* and *12*, which were marked at the farthest distance from the heated surfaces. Temperature changes at the 1.85 m and 2.2 m were influenced by the distance grids. In those pictures two temperature drops could be seen, which occurred due to the influence of the distance grids. The velocity of the flow increased before the distance grid and the colder coolant mixed with the hotter one decreasing the temperature of the main flow. There was no temperature decrease near the central rod at the point *1*, where the flow cross section area was minimal; therefore, the temperature constantly increased until the saturation temperature.

Fig. 7 demonstrates a steam mass fraction change at the height 1750 – 2450 mm of the fuel channel.

The highest steam content was noticed at the point where the coolant temperature reached the saturation temperature primarily. The distance grids influenced on the rise of the steam content, however, the highest partial increase was noticed just after the grid. The further overall steam mass fraction was reduced due to the flow contact with the colder coolant which passed the distance grid. The steam generation rose due to the release of the heat from the fuel elements in the segments between the two adjacent grids. Only at the point *7*, a reduction of the steam content was noticed. The main reason for that was a local increase of the pressure and a decrease of the temperature at the point *7*, therefore, the heat release from the fuel elements was not sufficient for the steam generation. The steam fraction augmentation directly at the grid was influenced by the increase of the coolant velocity and decrease of the pressure (Fig. 9).

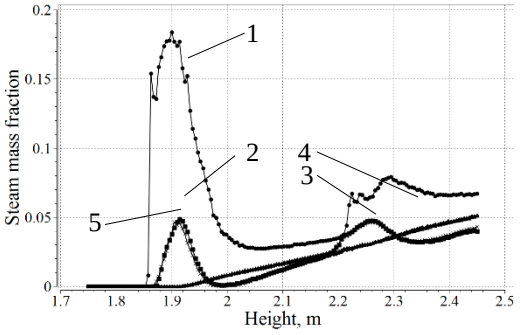

a

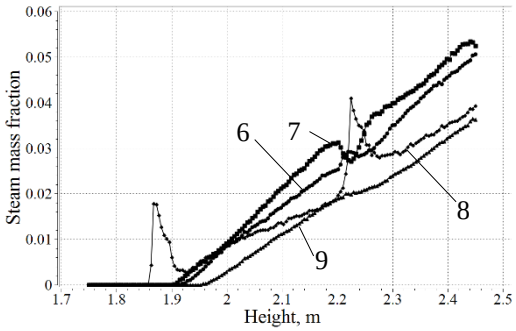

b

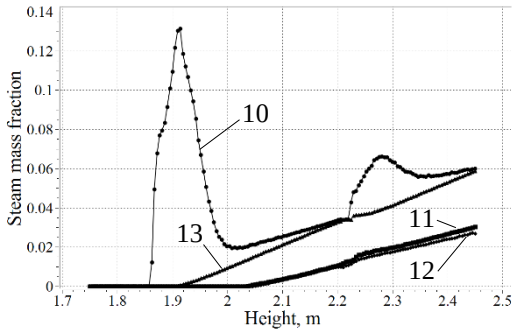

c

Fig. 7 Steam mass fraction change along the fuel channel: (a) at the *1 – 5* points; (b) at the *6 – 9* points; (c) at the *10 – 13* points

Fig. 8 presents the coolant velocity change at the height 1750 – 2450 mm of the fuel channel.

The slight alteration of the velocity was influenced by the coolant density change in the region where the coolant temperature was lower than the saturation temperature. The further more rapid augmentation of the velocity was affected by the steam generation (two-phase flow). The highest velocity was observed at the grids where the cross section area of the coolant flow was lower. The velocity was reduced after passing the grid where the cross section area increased and the coolant was mixed up with the colder coolant. Velocity disturbances could be observed in some points after the distance grids. The perturbations occurred due to the decrease of the steam content in the area behind the distance grid. It was noticed, that the cases where the steam fraction was highest in the distance grid corresponded to the cases where the highest decrease of the velocity behind distance grid was observed.

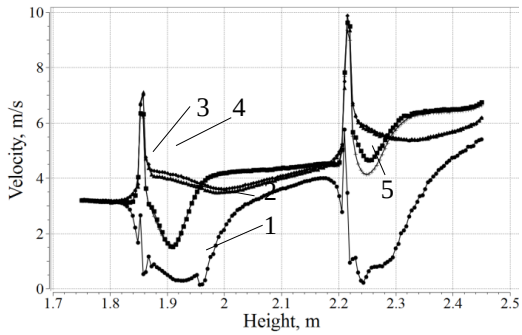

a

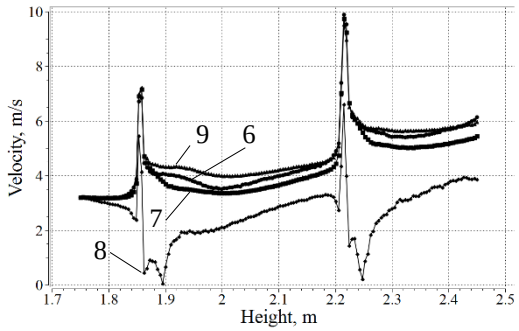

b

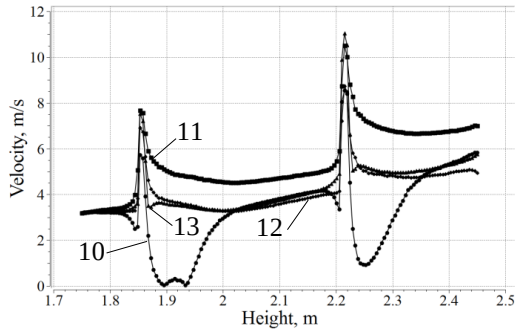

c

Fig. 8 Velocity change along the fuel channel: (a) at the *1 – 5* points; (b) at the *6 – 9* points; (c) at the *10 – 13* points

Fig. 9 represents a coolant pressure change at the height 1750 – 2450 mm of the fuel channel.

The alteration of the coolant pressure was influenced by the same factors as the changes of the coolant velocity. The reduction of the pressure was insufficient in the region where the single phase flow (without boiling) took place. The augmentation of the velocity had an influence on the pressure decrease in the zone where the steam generation started and proceeded. The pressure increase just before the grid was influenced by the flow compression before the obstruction (spacer).

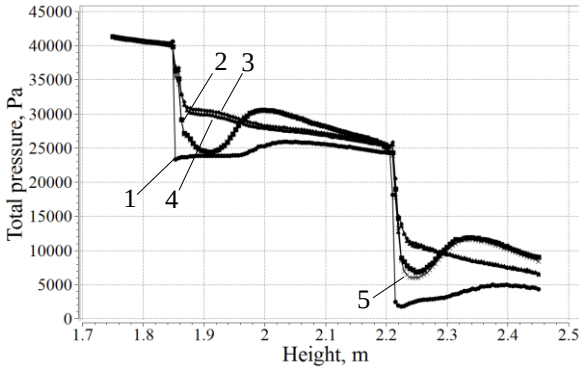

a

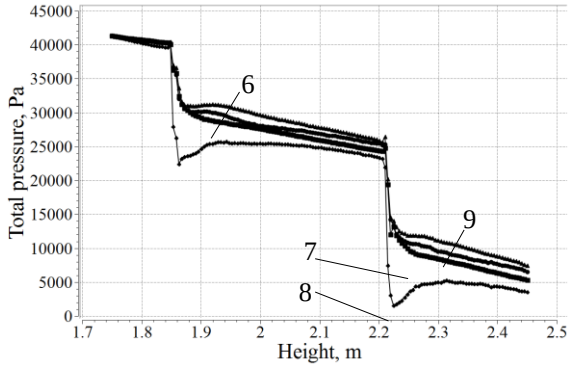

b

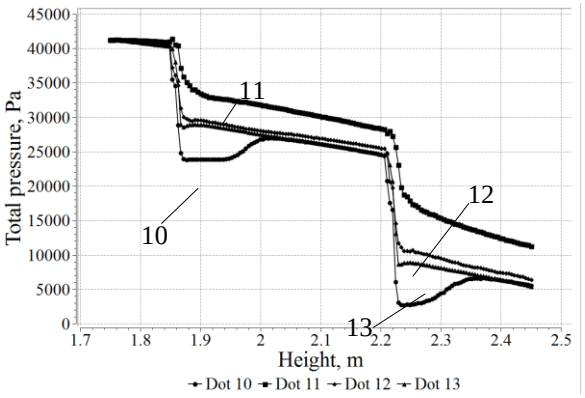

c

Fig. 9 Pressure change along the fuel channel: (a) at the *1 – 5* points; (b) at the *6 – 9* points; (c) at the *10 – 13* points

Fig. 10 shows the distribution of the heat transfer coefficient along the lower part of the fuel channel. The average value of the heat transfer coefficient was equal to 25000 W/(m^2·K) approximately. The heat transfer coefficient sharply increased at the places where the distance grids were mounted because of the reduction of the free cross sectional area of the channel and augmentation of the flow velocity there. Generation of the steam (two phase flow) had reduced the resistance at the second spacer and therefore the heat transfer coefficient was lower (second peak) than for the single phase flow at the first spacer (first peak).

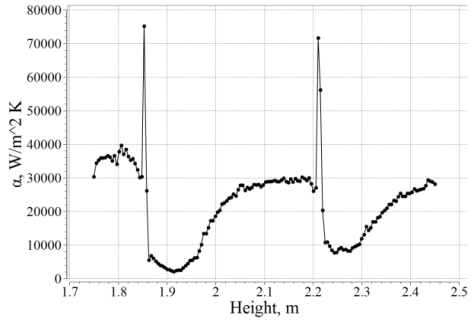

Fig. 10 Heat transfer coefficient distribution along the lower part of the fuel channel at the 1.75 – 2.45 m height

3. Coolant flow parameters variation across the fuel channel

Figs. 11 – 15 and Fig. 16 represent a variation of the thermal and hydro dynamical parameters at the different cross sections of the lower part of the fuel channel.

Fig. 11 shows the distribution of coolant's temperature across the fuel channel at the height equal to 2.395 m (channel without spacer) and 2.404 m (channel with spacer).

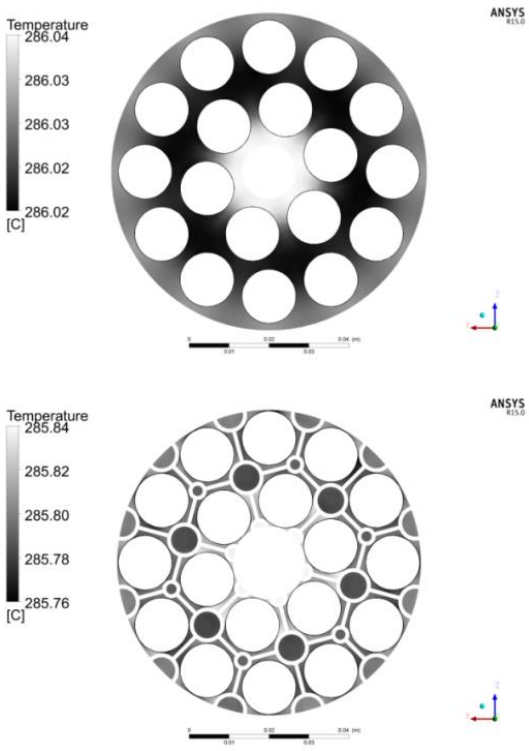

Fig. 11 Coolant temperature distribution across the fuel bundle: top – fuel channel without spacer; down – with spacer

The maximum temperature (286°C) was observed nearby the central rod of the fuel assembly in the channel without the obstacle (spacer) because of the minimal coolant's flow cross section area and the large contact surface

between the coolant and the fuel rods. The coolant temperature was the lowest at the area between the first and the second circles of the fuel rods due to the maximal cross area of the coolant flow there and the lowest pressure. The right part of Fig. 11 shows a situation when the coolant streamed through the distance grid. Similar like in the case without obstacles, the maximum temperature of the coolant was reached nearby the central rod in the channel with spacer. The average temperature in the cross sectional area was a bit higher for the case with the spacer (285.9°C) than for the case without the spacer (285.7°C).

Fig. 12 shows a steam mass fraction distribution across the fuel channel. The maximum steam mass fraction was observed at the central part of the fuel channel (near the central rod) because of the highest temperature of the coolant and therefore the earliest generation of the steam. The steam mass fraction was lower and uneven between the first and the second circles of the fuel rods. It was higher in the area between the three fuel rods (smaller cross section) than in the area between four fuel rods (larger cross section).

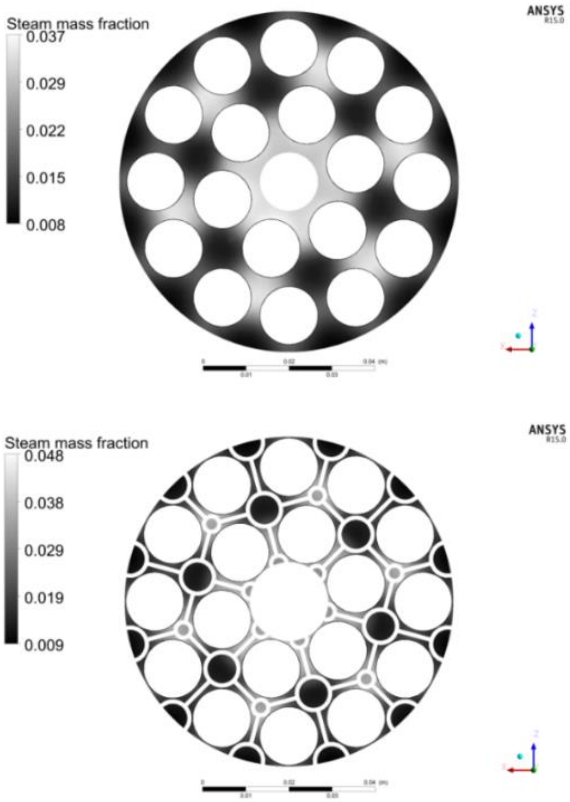

Fig. 12 Steam mass fraction distribution across the fuel bundle: top – fuel channel without spacer; down – with spacer

Fig. 13 shows the coolant flow at the same cross section of the lower part of the fuel assembly as it was presented in Fig. 12. It can be noticed that the coolant run from the periphery of the channel to the central part of the fuel assembly. Moreover, the coolant, carrying steam, flowed from the region between the first and the second cycles of the fuel rods towards the central part. Therefore, a steam mass fraction became the highest around the central rod.

Fig. 14 presents a coolant velocity distribution before the distance grid in the lower part of the fuel assembly.

The lowest velocity was observed at the periphery of the channel and near the central rod.

Fig. 15 shows a coolant total pressure distribution before the distance grid in the lower part of the fuel assembly. The minimum pressure of the coolant was observed at the same places where the velocity of the coolant was the highest (Fig. 14).

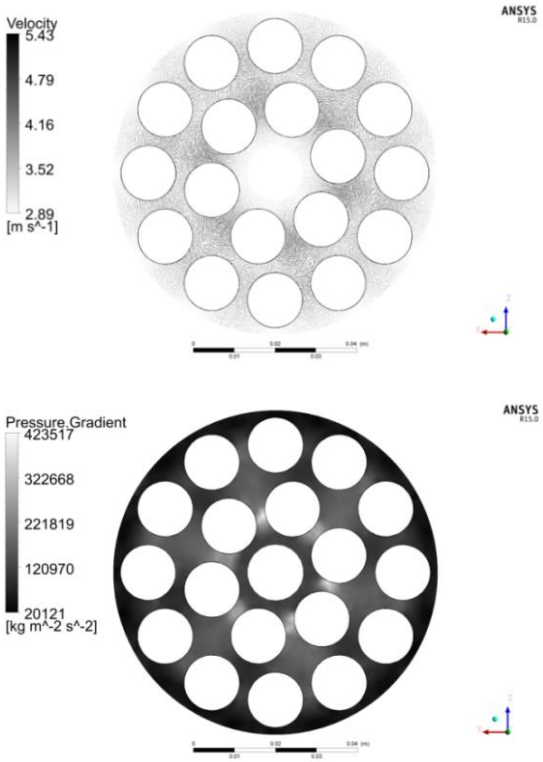

Fig. 13 Coolant flow in the lower part of the fuel assembly

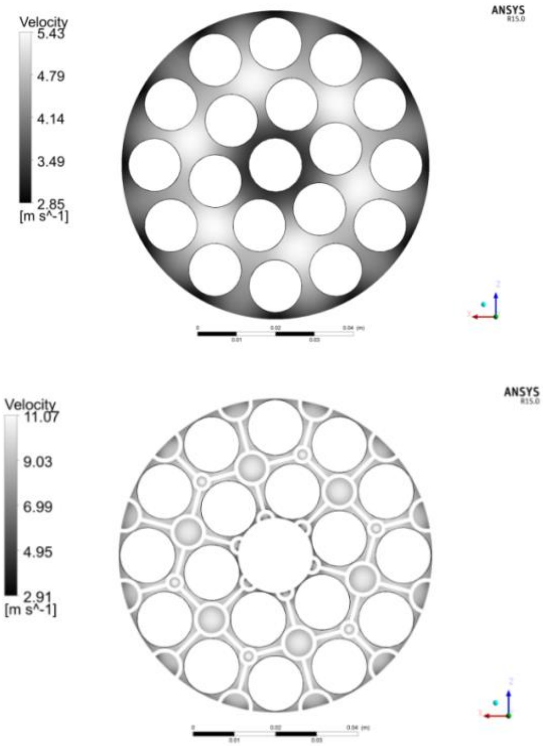

Fig. 14 Coolant velocity distribution across the fuel bundle: left – fuel channel without spacer; right – with spacer

Fig. 16 demonstrates steam mass fraction distribution in the different cross sections of the lower part of the fuel assembly, where the temperature of the coolant was close to the saturation temperature. It can be noticed that the steam generation started at the moment when the coolant flow crossed the spacer due to the local pressure drop in the grid. The water-steam coolant mixed with the single phase non-boiling coolant and, therefore, steam mass fraction was reduced after the grid (the first three cross sections in the Fig. 16). The further steam generation was determined by the heat release of the fuel elements.

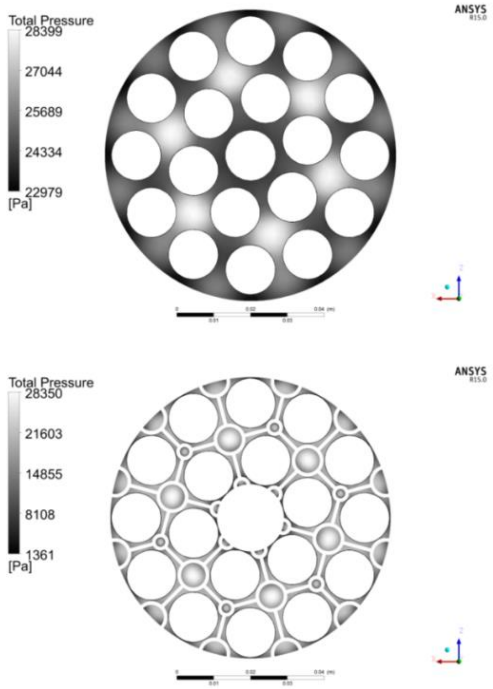

Fig. 15 Coolant pressure distribution across the fuel bundle: left – fuel channel without spacer; right – with spacer

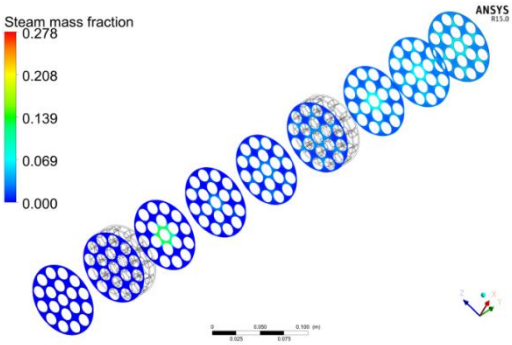

Fig. 16 Steam mass fraction distribution in the different cross sections of the lower part of the fuel bundle

4. Conclusions

It was observed that the pressure drop and change of the coolant's temperature were mainly determined by the irregular heat release. The pressure drop at the distance grids was the main reason for the rapid local steam generation.

The maximum temperature was observed nearby the central rod of the fuel assembly in the channel without and with the spacers due to the minimum coolant's flow cross section area and a large contact surface between the coolant and the fuel rods. The coolant's temperature was the lowest at the area between the first and the second circles of the fuel rods due to the maximal cross section area of the coolant flow there and the lowest pressure.

The coolant's flow direction was from the periphery to the region between the first and the second rods cycles and further – towards the central part of the fuel assembly. The slight change of the velocity in the region where coolant temperature was lower than the saturation temperature was influenced by the coolant density change. The further more rapid augmentation of the velocity was affected by the steam generation. The highest velocity was observed at the grids where the cross section area of the coolant flow was lower. Velocity was reduced after passing the grid where the cross section area was increased and the coolant was mixed up with the colder flow.

The alteration of the coolant pressure was influenced by the same factors as the changes of the coolant velocity. The reduction of the pressure was insufficient in the region where the single phase flow (without boiling) took place. The augmentation of the velocity influenced on the pressure decrease in the zone where the steam generation started and proceeded. The pressure increase just before the grid was influenced by the flow compression before the obstruction (spacer).

The distance grids influenced on the rise of the steam content, however, the highest increase was observed just after the grid. The local steam fraction augmentation directly at the grid's frame was influenced by the increase of the coolant's velocity and a local pressure drop there. The further water-steam coolant was mixed with the single phase non-boiling coolant and therefore steam mass fraction was reduced. Hereafter, steam generation was determined by the heat release of the fuel elements. The maximum steam mass fraction was at the central part of the fuel channel (near the central rod) because of the highest temperature of the coolant and, therefore, the earliest generation of the steam. The steam mass fraction was lower and uneven between the first and the second circles of the fuel rods.

The average value of the heat transfer coefficient was equal to 25000 W/(m^2·K) approximately. The heat transfer coefficient sharply increased at the places where the distance grids were mounted due to the reduction of the free cross sectional area of the channel and the augmentation of the flow velocity there. The generation of the steam reduced the resistance at the second distance grid and, therefore, the heat transfer coefficient was less here than for the single phase flow at the first distance grid.

References

1. **Almenas, K.; Kaliatka, A.; Ušpuras, E.** 1998. Ignalina RBMK – 1500. A Source Book. – Kaunas: Lithuanian Energy Institute, 198 p.
2. **Abramov, M.I.; Avdeev V. I.; Adamov E. O.** and al. 2006. Channel type nuclear energy reactor RBMK – 1000. – GUP NIKIET, 632 p. (in Russian).
3. **James, H. Rust.** 1979. Nuclear Power Plant Engineering Haralson Publishing Company, 504 p.
4. Boiling Water Reactor Systems – NRC www.nrc.gov/reading-rm/basic-ref/teachers/03.pdf.

5. **Stravinskas, S.; Pashkevichius, G.; Krivov, I.; Krivoshein, G.** Equipment for repair of the RBMK-1500 fuel assemblies of Ignalina NPP. http://www.dysnai.org/Reports/2000.
6. **Hassan, Y.A.** 2008. Computational Fluid Dynamics for Natural Circulation: Needs & Verification and Validation. IAEA Course on Natural Circulation in Water-Cooled Nuclear Power Plants, International Centre for Theoretical Physics (ICTP), Trieste, Italy, Paper ID. T27 and T28.
7. **Ušpuras, E.; Kaliatka, A.** 2006. Accident and transient processes at NPP's with channel - type reactors, Lithuanian Energy Institute, Kaunas.
8. **Skalozub, V.; Kim, V.** 2002. Thermohydrodynamic models adequacy assessment methods within the frameworks of a calculation means verification/validation program for accident processes analysis, Nuclear and radiation safety 1: 57-76.
9. **Ustinenko, V.; Samigulin, M.; Ioilev, A.; Lob, S.; Tentner, A.; Lychagin, A.; Razin, A.; Girin, V.; Vanyukov, Ye.** 2008. Validation of CFD-BWR, a new two-phase computational fluid dynamics model for boiling water reactor analysis, Nuclear Engineering and Design 238: 660-670. https://doi.org/10.1016/j.nucengdes.2007.02.046.
10. **Kurul, N.; Podowski, M.Z.** 1990. Multi-dimensional effects in sub-cooled boiling, In: Proc. 9th Heat Transfer Conference, Jerusalem.
11. **Liu, T.J.** 1998. The role of bubble size on liquid phase turbulent structure in two-phase bubbly flow, In: Proc. Third International Congress on Multiphase Flow ICMF'98, Lyon, France, June 8–12, CD ROM Publication.
12. **Lee, T.H.; Park, G.C.; Lee, D.J.** 2002. Local flow characteristics of subcooled boiling flow of water in a vertical annulus, International Journal of Multiphase Flow 28: 1351–1368. https://doi.org/10.1016/S0301-9322(02)00026-5.
13. **Lo, S.** 2005. Modelling multiphase flow with an Eulerian approach, Von Karman Institute Lecture Series—Industrial Two-Phase Flow CFD, May 23–27, von Karman Institute, Belgium.
14. **Ohnuki, A.; Akimoto, H.** 2001. Model development for bubble turbulent diffusion and bubble diameter in large vertical pipes, Journal of Nuclear Science and Technology 38: 1074-1080. http://dx.doi.org/10.1080/18811248.2001.9715138.
15. **Serizawa, A.; Kataoka, I.; Michiyoshi, I.** 1975. Turbulent structure of air-water bubbly flow, Parts I-III, International Journal of Multiphase Flow 2: 221–259. http://dx.doi.org/10.1016/0301-9322(75)90011-7.
16. **Wang-Kee In, Dae-Hyun Hwang, Jae Jun Jeong.** 2013. A subchannel and CFD analysis of void distribution for the BWR fuel bundle test benchmark, Nuclear Engineering and Design 258: 211-225. http://dx.doi.org/10.1016/j.nucengdes.2013.02.006.
17. **Krepper, E.; Koncar, B.; Egorov, Y.** 2007. CFD modelling of subcooled boiling-Concept, validation and application to fuel assembly design, Nuclear Engineering and Design 237(7): 716-731. http://dx.doi.org/10.1016/j.nucengdes.2006.10.023.
18. **Yang, S. K.; Chung, M. K.** 1998. Turbulent flow through spacer grids in rod bundles, Journal of Fluid Engineering 120: 786-791. http://dx.doi.org/10.1115/1.2820739.
19. **Caraghiaur, D.; Frid, W.; Tilmark, N.** 2004. Detailed pressure drop measurements in single-phase adiabatic air-water turbulent flows in realistic BWR fuel assembly geometry with spacer grids, 6th International Conference on Nuclear Thermal Hydraulics, Operations and Safety (NUTHOS-6) Nara, Japan, October 4-8, 2004.
20. **Caraghiaur, D.; Anglart, H.; Frid W.** 2009. Experimental investigation of turbulent flow through spacer grids in fuel rod bundles, Nuclear Engineering and Design, 239(10): 2013-2021. http://dx.doi.org/doi: 10.1016/j.nucengdes.2009.05.029.
21. CFX. Innovative turbulence modelling: SST model in ANSYS CFX, Technical report, ANSYS Ltd, 2006.
22. ANSYS CFX Solver Theory Guide. Release 12.0. 2009. ANSYS Inc. Southpointe. McCormick, Barnes 1979.
23. SolidWorks®3D mechanical CAD software. 1995-2011, Dassault Systèmes SolidWorks Corporation, a Dassault Systèmes S.A. company, 300 Baker Avenue, Concord, Mass. 01742 USA. All Rights Reserved.
24. **Krepper, E.; Končar, B.; & Egorov, Y.** 2007. CFD modelling of subcooled boiling—Concept, validation and application to fuel assembly design, Nuclear Engineering and Design, 237(7): 716-731. http://dx.doi.org/10.1016/j.nucengdes.2006.10.023.
25. **Fedaravičius, A.; Jonevičius, V.; Kilikevičius, S.; Paukštaitis, L.; & Šaulys, P.** 2011. Estimation of the Drag Coefficient of Mine Imitator in Longitudinal Air Flow Using Numerical Methods, Transport, 26(2): 166–170. http://dx.doi.org/10.3846/16484142.2011.589427.

L. Paukštaitis, S. Kilikevičius, J. Gudzinskas, M. Gylys, V. Lukoševičius

NUMERICAL ANALYSIS OF THERMAL AND HYDRO DYNAMICAL PROCESSES IN LOWER FUEL CHANNEL PART OF BOILING WATER REACTOR

S u m m a r y

This article presents results of a 3D numerical analysis of the thermal and hydro dynamical processes which take place inside the fuel channel of the RBMK-1500 reactor during interaction between coolant and fuel assembly.

The simulation was made using ANSYS CFX code in order to evaluate coolant's pressure, temperature, flow velocity and steam mass fraction changes at the distance grids (spacers) and at the heat transfer intensification grids (intensifiers) along and across the fuel channel.

The obtained results help better to understand the processes which have a direct influence on the reactor safety. Information about the peculiarities of steam generation process inside the fuel channel (temperature change, pressure drop, flow velocity, steam mass fraction) enables to identify the most loaded points of the fuel channel.

Keywords: fuel channel; coolant temperature; velocity; pressure drop; steam fraction; spacer; intensifier.

Received October 17, 2016
Accepted October 13, 2017